Tensile failure strength and separation angle of FDM 3D printing PLA material: experimental and theoretical analyses

Tianyun Yao[a,b], Juan Ye[a,b], Zichen Deng[a,b,*], Kai Zhang[a,b,], Yongbin Ma[a,b], Huajiang Ouyang[c]**

[a] School of Mechanics, Civil Engineering and Architecture, Northwestern Polytechnical University, Xi'an 710072, P. R. China

[b] MIIT Key Laboratory of Dynamics and Control of Complex Systems, Northwestern Polytechnical University, Xi'an 710072, P. R. China

[c] School of Engineering, University of Liverpool, Liverpool L69 3GH, UK

* Corresponding author.

** Corresponding author.

E-Mail address: dweifan@nwpu.edu.cn(Zichen Deng); kzhang@nwpu.edu.cn(Kai Zhang)

Abstract

It is discovered in this investigation that there exist two different failure modes and a special separation angle which is the demarcation point of the two different failure modes when FDM (Fused Deposition Modelling) 3D printing materials fail under a tensile load. In order to further understand the mechanical properties of FDM 3D printing materials and promote the use of FDM 3D printing materials, their tensile failure strengths at different printing angles and separation angles are measured and analysed theoretically. A new separate-modes of transversely isotropic theoretical failure model is established to predict the tensile failure strength and separation angle of FDM 3D printing PLA (polylactic acid) material based on the hypothesis of transverse isotropy and the classical separate-modes failure criterion. During this research, the tensile specimens designed according to the current test standard ISO (527-2-2012) for plastic-multi-purpose specimens are fabricated in 7 different printing angles (0°, 15°, 30°, 45°, 60°, 75°, 90°) and three levels of printing layer thickness (0.1 mm, 0.2 mm, 0.3 mm). Experimental results show that the tensile failure strength increases with the increase of the printing angle or the decrease of the layer thickness. Meanwhile, inter-layer failure tends to occur when the printing angle is small and in-layer failure tends to occur when the printing

angle is big. In comparison with the results predicted by the established theoretical model, all values of the Generalized-Relative-Root-Mean-Square Error are close to zero and the experimental separation angles are also between 45° and 60°. So the predictive capacity of the theoretical model is affirmed by experimental results.

Graphical Abstract

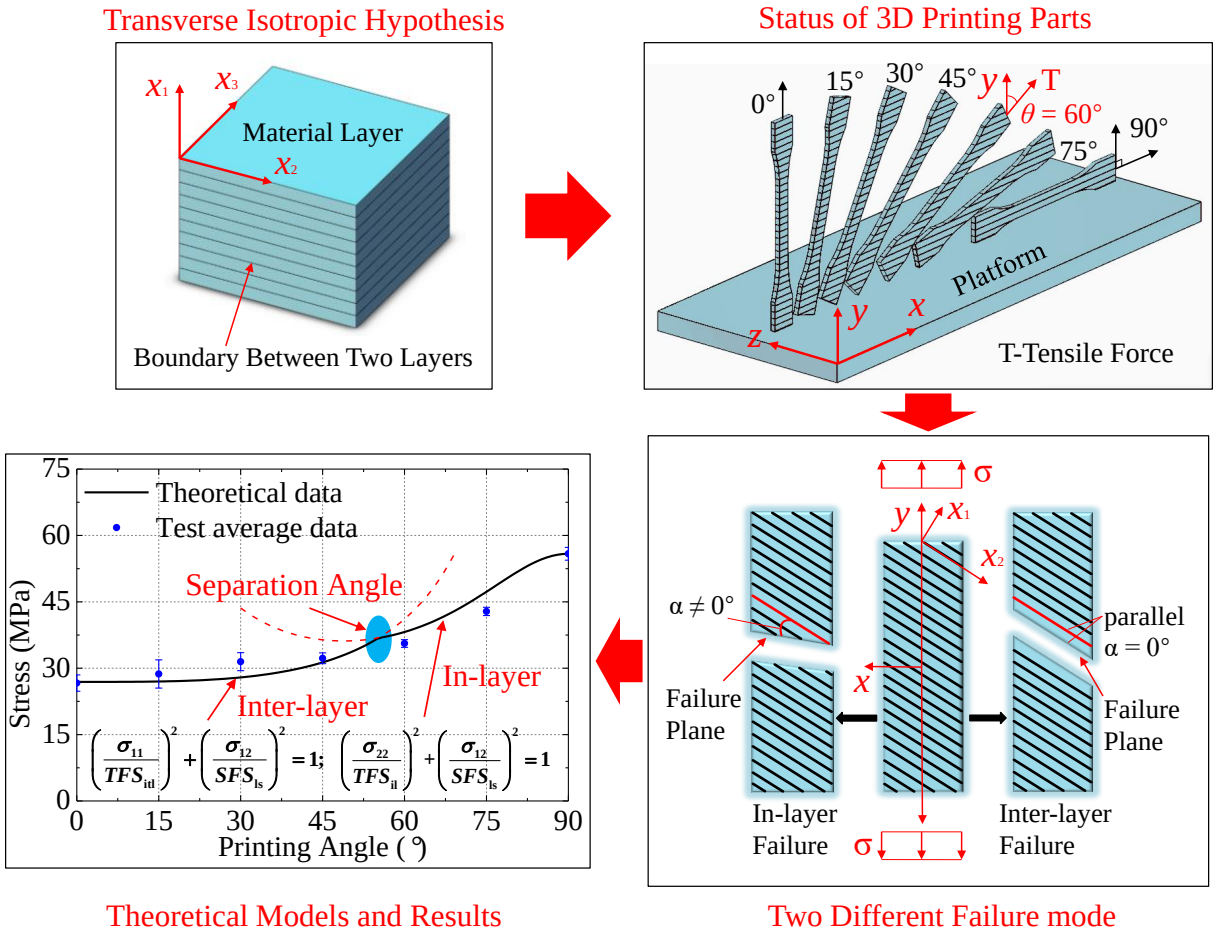

Keywords: 3D printing; tensile failure strength; separation angle; failure criterion; printing angle; layer thickness

1. Introduction

One area of great progress in manufacturing science and engineering is the rapid development of 3D printing technology in the past two decades [1-4]. Combining Computer Aided Design (CAD) and Computer Aided Manufacturing (CAM) technologies, 3D printing technology fabricates items without involving any traditional cutting techniques and the waste of raw materials caused in this process is also very little [5, 6]. For manufacturing thin-walled

structures, complex structures [7, 8] and multi-material structures [9, 10], this technology has inherent advantages [11-13]. Nowadays, 3D printing technology has been widely applied in manufacturing [14], civil engineering [15, 16], automotive engineering [17], biomedical engineering [18-21], food [22-24], clothing [25] and so on.

Fused Deposition Modelling (FDM) is a widely-used 3D printing technology for polymer and composite filaments due to its flexible and rapid printing process, low cost, diversity and non-toxicity of materials, high strength and toughness of materials. A schematic diagram of FDM 3D printing technology is shown in Fig. 1 and the printing process can be described as follows. A digital 3D model should be built in CAD software and stored as a stereolithography (STL) format file. Then a slicing software module is used to slice the 3D model into thin layers horizontally and control the FDM machine. Printing parameters including printing speed, layer thickness, printing temperature, filling rate, printing orientation, support structure and so on are all set in the slicing software. During the modelling process, a printing filament is extruded into the nozzle at semi-liquid state and deposited onto the previous material layer shown in Fig. 1. After the new material layer solidifies on the printing object at room temperature, the printing platform with the printing item moves down by the height of one material layer and then the next material layer will be printed. This process will continue until the entire model has been printed. At last, the support structure will be removed manually. Considering the fabrication process, a FDM 3D printing item can be simplified as a transversely isotropic material and the plane of transverse isotropy is the material layer plane.

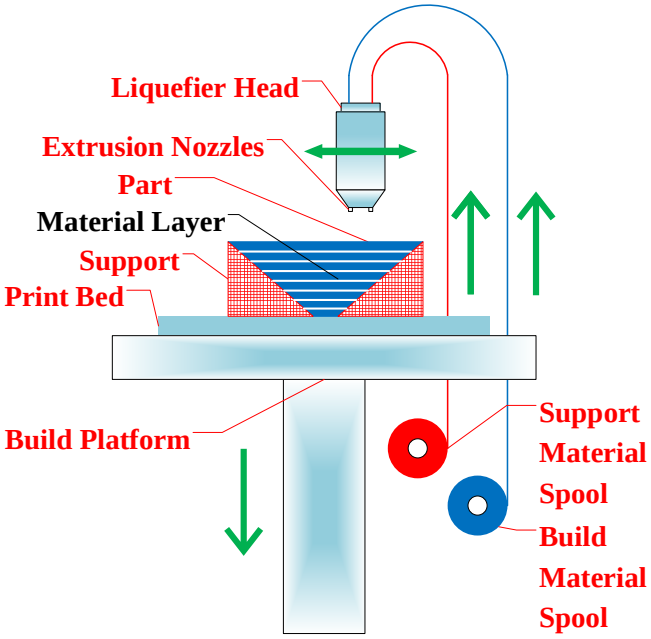

Fig. 1. Schematic diagram of FDM 3D printing technology.

As a new fabricating process for a new class of materials, one shortcoming of this 3D printing technology is that the mechanical properties are still unclear, and the constitutive models and strength models dedicated for FDM 3D printing materials are not yet available. Thus actual FDM 3D printing structures cannot be modelled and analysed accurately. This lack of knowledge has seriously hindered the development and application of FDM 3D printing technology and calls for its research. The research on the mechanical properties of FDM 3D printing materials has mainly focused on two aspects: failure strengths [26] and elastic properties. Among them, there has been more research on their elastic properties. However, the research on their failure strength is still rare.

The research on failure strength of 3D printing materials can be roughly divided into 3 categories. Qualitative parametric analysis is the first and most common one. Chacón et al. [27] did tests and analysed the influences of parameters including building orientation, layer thickness and feed rate on the tensile strength and bending strength. They found that layer thickness and feed rate had a negative correlation with the two strengths. On the other hand, building orientation had an obvious influence on the two strengths. Tanikella et al. [28] investigated the tensile strength for a wide range of 3D printing materials. The results demonstrated that the tensile strength of 3D printing specimens depended largely on the mass of the specimen, for all materials. Sood et al. [29] evaluated the relationship between the

parameters including layer thickness, orientation, raster angle, raster width and air gap and tensile, flexural and impact strength. Empirical models relating mechanical responses and process parameters were developed. Croccolo et al. [30] studied the effects of FDM production parameters on the tensile failure strength and the stiffness of the materials. An empirical analytical model was developed based on the process parameters. García-Plaza et al. [31] established a mathematical modelling to analyse the effect of printing parameters including building orientation, layer thickness, feed rate, and plate-extruder movements on the dimensional accuracy, flatness error, and surface texture of 3D printing PLA parts. Other parametric analyses [32-37] have also been done in the past decades. All of the above studies mainly focused on the influences of printing parameters on failure strength of 3D printing materials. Only some empirical models and qualitative results were obtained during these research.

Secondly, some theoretical failure models have been built to predict the failure strength of 3D printing materials. Zhang et al. [38] established a theoretical model based on Tsai-Wu failure criterion [39] to predict the macroscopic failure of 3D printing glassy polymers and the model was applied to simulate the failure of 3D printing lattice structures. Ahn et al. [40] developed an anisotropic failure model of tensile strength as a function of raster angle by Tsai-Wu failure criterion [39]. A failure criterion for anisotropic materials that incorporated stress interactions was implemented to predict the failure strength of 3D printing materials by Obst et al [41]. Theoretical results showed that the failure of 3D printing parts was strongly influenced by the interaction between stresses and there were significant differences between tensile and compressive strengths. The theoretical failure models mentioned above only have the ability to roughly represent the experimental data without considering the specific experimental phenomena.

Thirdly, the strength of multi-materials and structures fabricated by 3D printing technology has also been investigated. Ning et al. [42] experimentally researched the effect of raster angle, infill speed, nozzle temperature and layer thickness on the tensile strength of carbon fibre-reinforced plastic composites (CFRP). These 4 factors had a significant impact on the tensile strength of CFRP. Caminero et al. [43] investigated the effect of graphene nanoplatelet reinforcement on the mechanical properties, dimensional accuracy, and surface texture of 3D

printed PLA structures. The 3D printed PLA-Graphene composite samples showed higher tensile strength, flexural strength, and inter-laminar shear strength than 3D printed PLA, and PLA 3D850 samples. Ulu et al. [44] experimentally studied the influence of printing orientation on the performance of 3D printing structures. An optimization algorithm was used to identify the build orientation that maximized the factor of safety (FS) of a structure under prescribed loading and boundary configurations.

Obviously, two problems exist in the previous research. Firstly, only qualitative results have been obtained in most previous parametric analyses of FDM 3D printing materials. Meanwhile, the empirical models constructed are rarely based on a mechanics principle. Secondly, theoretical models were only established on rough experimental phenomena and did not clearly classify the tensile failure modes of these materials. An accurate prediction of tensile failure strength (TFS) is very important for analysing the structures fabricated by FDM 3D printing technology, for the sake of structural safety. In order to promote and develop the 3D printing technology, a quantitative theoretical failure model which is consistent with experimental phenomena and based on experimental data is urgently needed.

A large number of experimental results obtained during this investigation demonstrate that there are two different failure modes, inter-layer failure mode and in-layer failure mode, when the FDM 3D printing PLA material fail. In addition, a special separation angle which is the demarcation point of the two different failure modes exist during the failure experiment. Therefore, a separate-modes of transversely isotropic theoretical failure model is established to predict the TFS and separation angle of the FDM 3D printing PLA material based on the hypothesis of transverse isotropy and classical separate-modes failure criterion [45]. The influence of printing angles and layer thickness on TFS is measured and analysed by tensile experiments and the parameters of the theoretical model is amended and improved based on the test data. At last, a modified theoretical failure model is obtained which can accurately predict the TFS with different printing angles and layer thickness and can approximately predict the range of the separation angle with different layer thickness.

The remainder of this paper is outlined as follows. Fabrication of specimens, tensile experiment and phenomena of experimental results are described in Section 2. The separate-modes of transversely isotropic theoretical failure model and the model in plane stress state are

established in Section 3. The detailed calculation process of separation angle show in Section 4. The approximate range of the separation angle and the TFS comparison between the theoretical data and experimental data have been analysed thoroughly in Section 5. Four conclusions of this paper are drawn in Section 6.

2. Procedures of experiment

2.1. Fabrication of 3D printing specimens

2.1.1. Material and 3D printing machine

The testing material used during this research is polylactic acid (PLA) which is an amorphous, durable, strong thermoplastic, healthy and pollution-free material with excellent printing capability. Therefore, it is one of the most commonly used materials in 3D printing. The PLA filaments used are produced by Polymaker Industries (Shanghai, China) and their properties are given in Table 1.

Table 1 Properties of PLA filament.

Property	Typical value
Average Filament Diameter (mm)	1.75 ± 0.05
Recommended Printing Temperature (°C)	195 ~ 230
Softening Temperature (°C)	146 ~ 150
Recommended Printing Speed (mm/s)	40 ~ 90
Density (g/cm^3 at 21.5 °C)	1.17 ~ 1.24
Recommended Heated Build Platform Temperature	Not Required

Desktop 3D printer (Makerbot Industries, Brooklyn, USA) is used to fabricate the test specimens. 3D printing software is used to control the printing parameters including printing angle, printing speed, temperature and so on. Printing temperature is set to 215 °C, which is suitable for the PLA filaments. The printable layer thickness is 0.05 ~ 1.2 mm. Considering the printing speed and mechanical properties, 3 levels of layer thickness are chosen in this research: 0.1 mm, 0.2 mm and 0.3 mm.

2.1.2. Printing dimension and states of specimens

The dimension of these 3D printing specimens follows ISO 527-2-2012 (International standard, plastics determination of tensile properties Part 2: Test conditions for moulding and extrusion plastics), which is shown in Fig. 2. The total number of specimens used during this research is 84 and the details are given in Table 2.

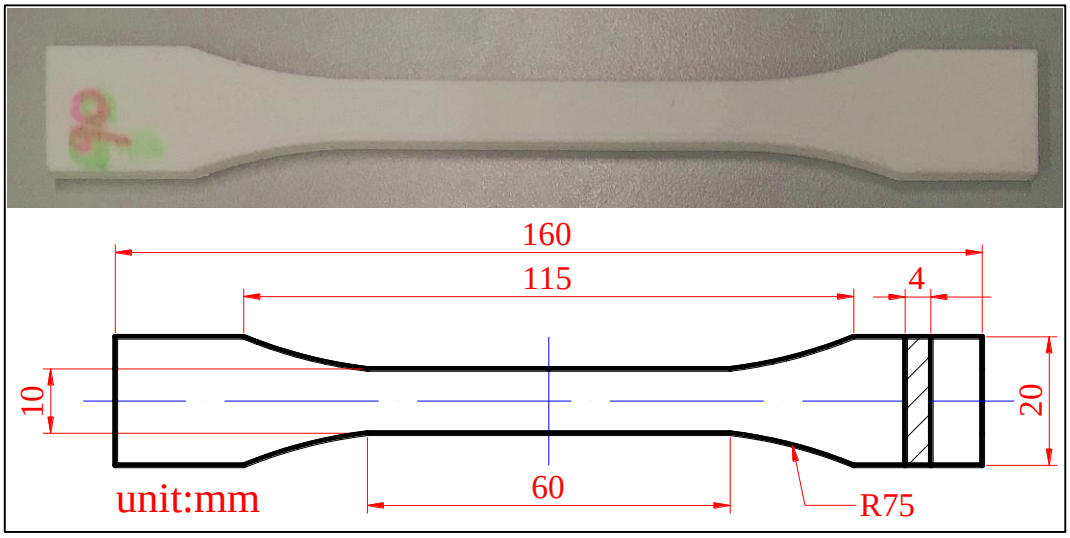

Fig. 2. The dimension of 3D printing specimens.

Table 2 The numbers of specimens used during this research.

Printing Angle (°)						
0	15	30	45	60	75	90
Layer thickness = 0.1 mm						
4	4	4	4	4	4	4
Layer thickness = 0.2 mm						
4	4	4	4	4	4	4
Layer thickness = 0.3 mm						
4	4	4	4	4	4	4

Based on previous research results and the forming process of FDM materials (layer by layer), the 3D printing material produced in this research project is modelled as being transversely isotropic. In order to understand the effect of printing angle on TFS of the material, these specimens are fabricated with 7 printing angles (2 angles of 0° and 90° for on-axis specimens; 5 angles of 15°, 30°, 45°, 60°, 75° for off-axis specimens), respectively. The

0° on-axis specimens are used to test the inter-layer TFS while the 90° on-axis specimens are used to test the in-layer TFS. Off-axis specimens are used to verify the new theoretical failure model established during this research. The printing states and printing angles are shown in Fig. 3. Here, the printing angle is defined as the angle between the direction that is perpendicular to the material layers and the direction of the tensile load to be applied onto the specimens in the tests. The hatched lines in Fig. 3 represent the boundary between two material layers.

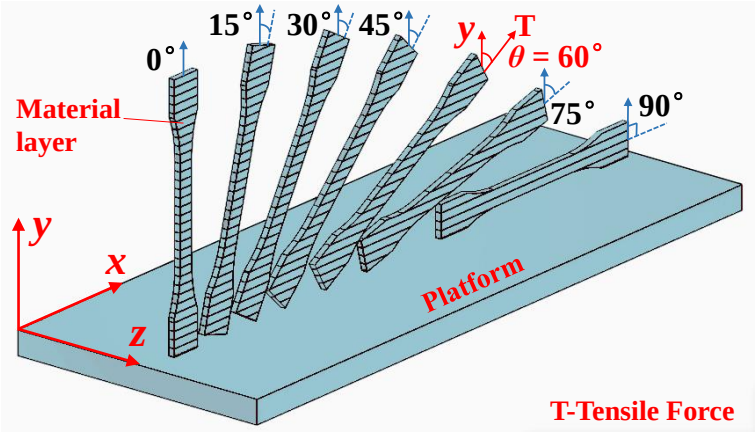

Fig. 3. The printing status and angles of specimens.

In order to ensure the printing quality of the specimens while considering the problem of excessively high hanging angle during the printing process, sufficient support structures are preset in the printing software. The support structures (SS) are illustrated in Fig. 4.

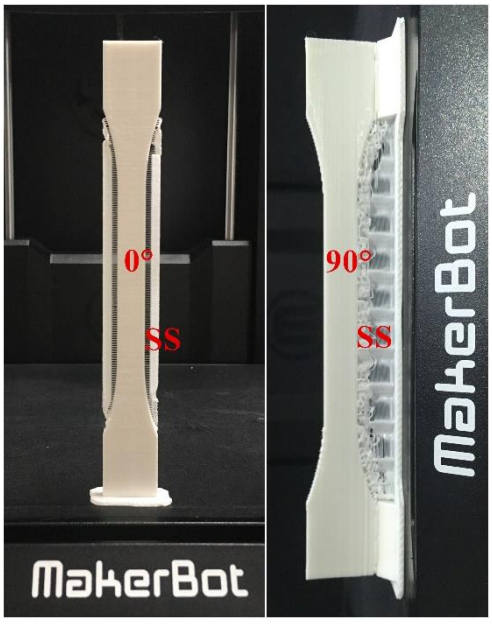

(a) Support structures of on-axis specimens.

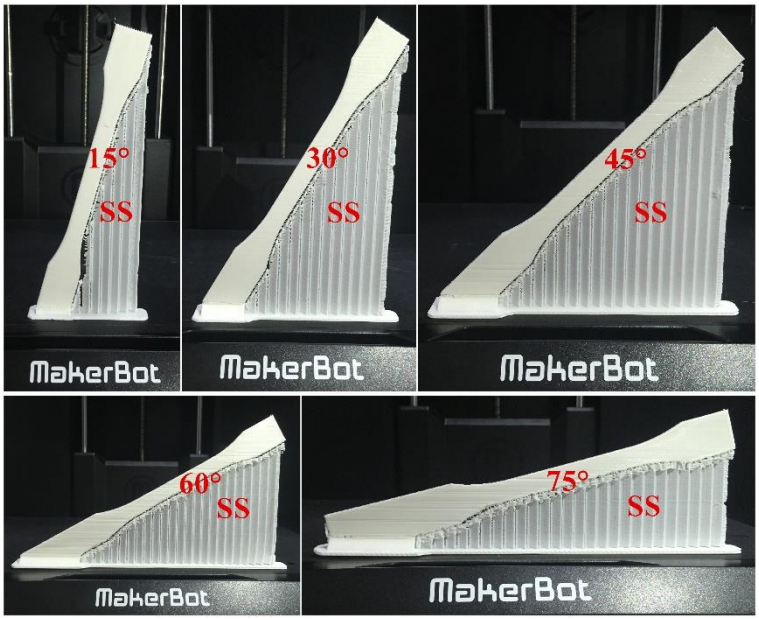

(b) Support structures of off-axis specimens.

Fig. 4. Support structures of 3D printing specimens.

2.2. Uniaxial tensile experiment of specimens

Quasi-static uniaxial tensile tests are performed on the computer-controlled electronic universal tensile machine provided by Changchun Institute of Mechanical Science China. In all the quasi-static tensile tests the specimens are stretched at a constant speed of 0.1 mm/min and at room temperature kept at 23 ℃. So the experiment condition is standard. The test machine and one of the specimens are shown in Fig. 5.

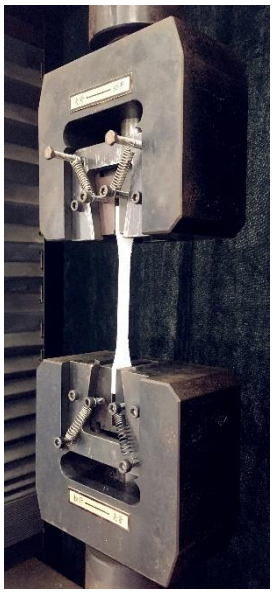

Fig. 5. The tensile machine and specimens under testing.

2.3. Phenomena of experimental results

Before analysing phenomena of the experiment results, two failure modes should be defined, inter-layer failure mode and in-layer failure mode, which are illustrated in Fig. 6. An inter-layer failure mode occurs when fracture appears at the interface between two adjacent material layers and the material layers remain intact after failure, and the angle α between the failure surface and the material layers is 0°. An in-layer failure mode occurs when material layers break and the angle α between the failure surface and the broken material layers is not equal to 0°.

Test results for 3 different layer thicknesses (0.1 mm, 0.2 mm, 0.3 mm) are shown in Fig. 7. All failure features are shown in an enlarged form. So both inter-layer failure mode and in-layer failure mode can be easily seen in this figure.

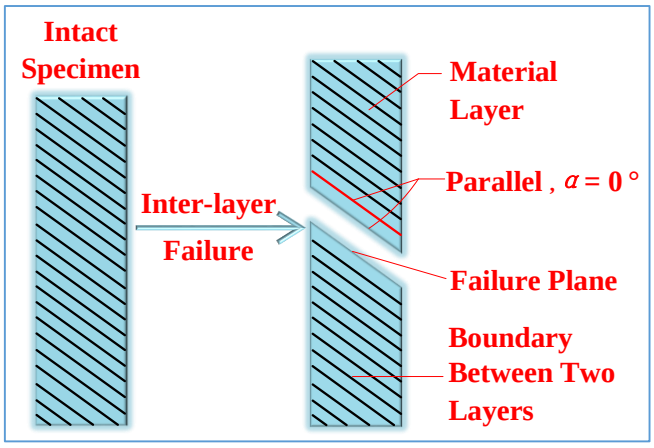

(a) Inter-layer failure mode.

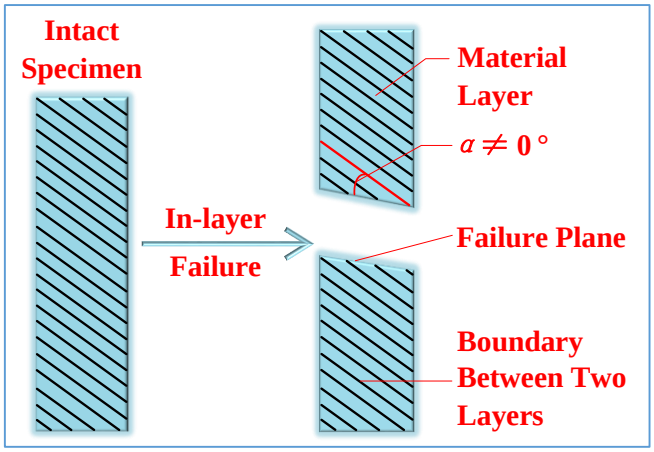

(b) In-layer failure mode.

Fig. 6. Schematic of inter-layer failure mode and in-layer failure mode.

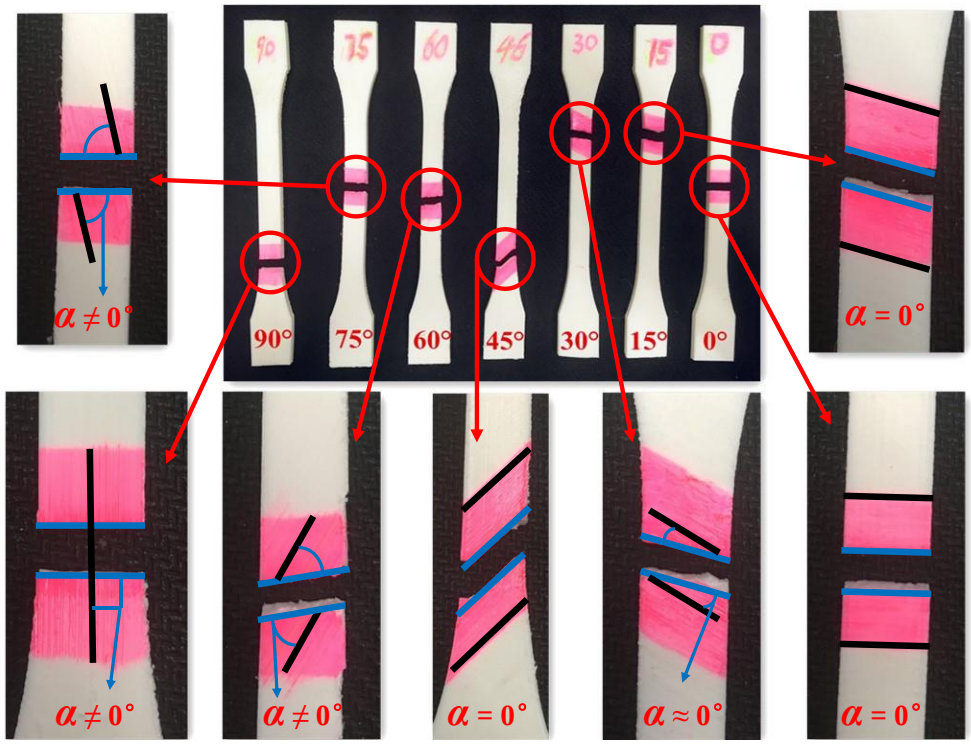

(a) Specimens with 0.1 mm layer thickness.

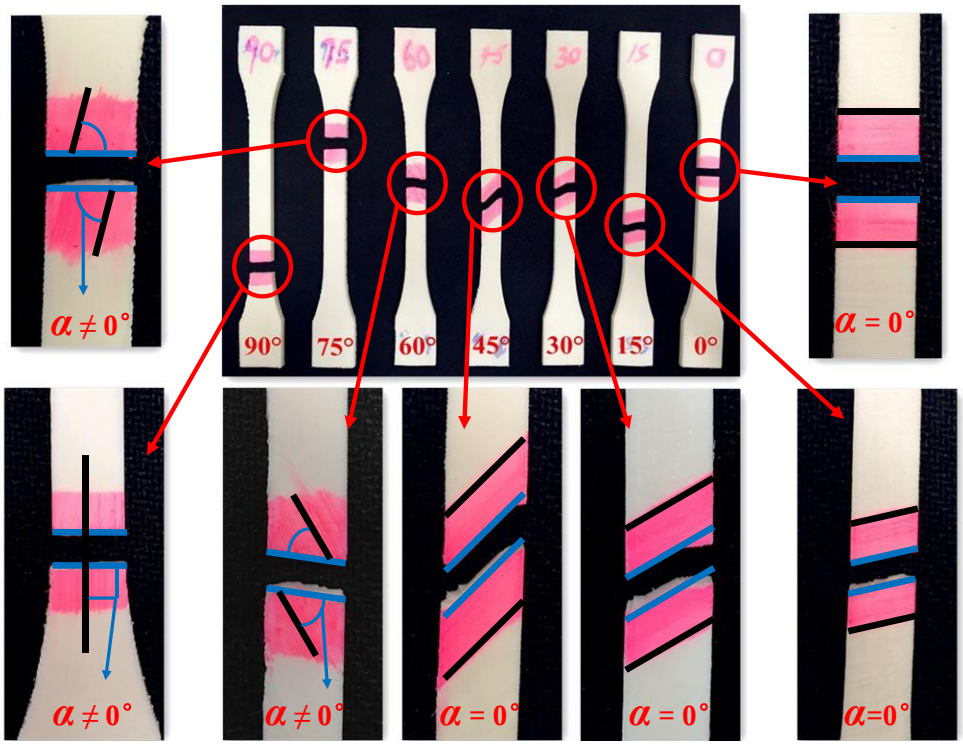

(b) Specimens with 0.2 mm layer thickness.

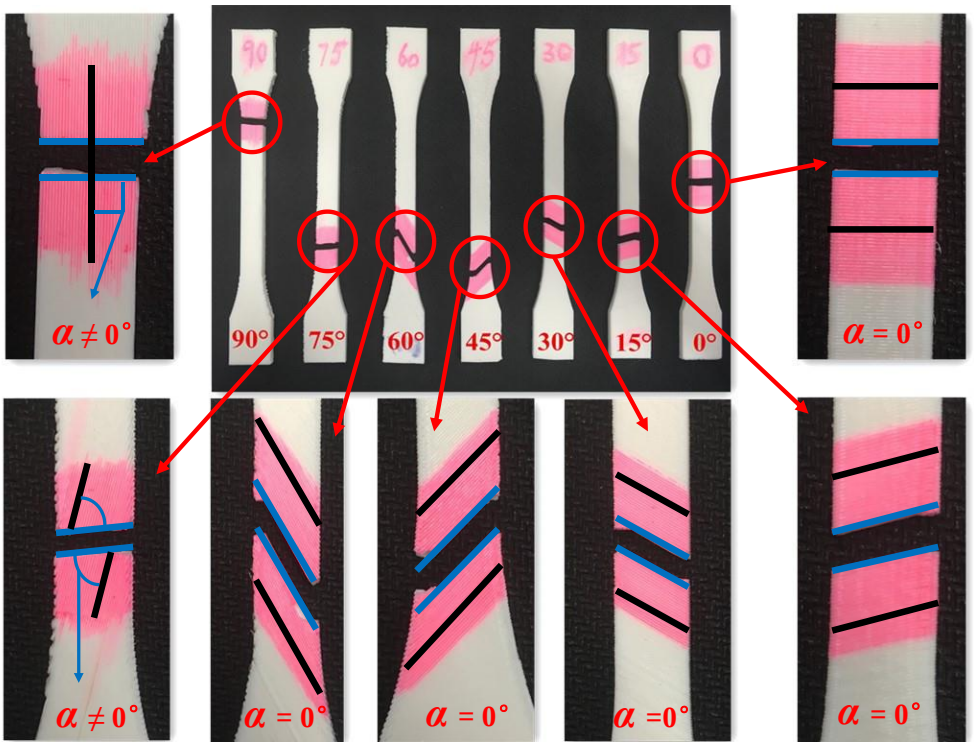

(c) Specimens with 0.3 mm layer thickness.

Fig. 7. Failure features and details of specimens with 3 different layer thicknesses.

3. Theoretical model

3.1. Separate-modes of transversely isotropic failure model

3.1.1. Quadratic failure model for transversely isotropic materials

Usually a quadratic failure criterion of isotropic materials is formulated in terms of the stress invariants. The invariants of stress tensor for isotropic materials are given below.

$$I_1^{\mathrm{i}} = \sigma_{11} + \sigma_{22} + \sigma_{33} \tag{1}$$

$$I_2^{\mathrm{i}} = \sigma_{11}\cdot\sigma_{22} + \sigma_{22}\cdot\sigma_{33} + \sigma_{33}\cdot\sigma_{11} - \sigma_{12}^2 - \sigma_{23}^2 - \sigma_{31}^2 \tag{2}$$

$$I_3^{\mathrm{i}} = \sigma_{11}\cdot\sigma_{22}\cdot\sigma_{33} + 2\sigma_{12}\cdot\sigma_{23}\cdot\sigma_{31} - \sigma_{11}\cdot\sigma_{23}^2 - \sigma_{22}\cdot\sigma_{31}^2 - \sigma_{33}\cdot\sigma_{12}^2 \tag{3}$$

where all the stresses in Eq. (1) ~ Eq. (3) are shown in Fig. 8. Superscript i in Eq. (1) ~ Eq. (3) represents isotropic materials.

As explained before, FDM 3D printing materials can be simplified as transversely isotropic materials with respect to the building direction of material layers. Here, a 3D rectangular

coordinate system is defined, with x_2 and x_3 being the two perpendicular axes in the plane of the material layers, and x_1 normal to this plane, as shown in Fig. 8. For transversely isotropic materials, the failure model must be invariant under any rotation of the x_2 and x_3 axes around x_1. Therefore, a function of stress invariants under rotation around x_1 is constructed for this special failure model. The stress invariants used in the special failure model can be expressed as follows.

$$I_1^{\mathrm{t\sim i}} = \sigma_{11} \tag{4}$$

$$I_2^{\mathrm{t\sim i}} = \sigma_{22} + \sigma_{33} \tag{5}$$

$$I_3^{\mathrm{t\sim i}} = \sigma_{23}^2 - \sigma_{22} \cdot \sigma_{33} \quad \text{or} \quad \frac{1}{4}\left(\sigma_{22} - \sigma_{33}\right)^2 + \sigma_{23}^2 \tag{6}$$

$$I_4^{\mathrm{t\sim i}} = \sigma_{12}^2 + \sigma_{13}^2 \tag{7}$$

$$I_5^{\mathrm{t\sim i}} = 2\sigma_{12} \cdot \sigma_{23} \cdot \sigma_{13} - \sigma_{22} \cdot \sigma_{13}^2 - \sigma_{33} \cdot \sigma_{12}^2 \tag{8}$$

Eq. (4) ~ Eq. (8) are obtained based on Eq. (1) ~ Eq. (3) and transverse isotropy. Superscript $\mathrm{t\sim i}$ in the Eq. (4) ~ Eq. (8) represents transversely isotropic materials.

The one-dimensional uniaxial TFS and shear failure strength (SFS) of FDM 3D printing materials are given below.

TFS_{itl} - the maximum of σ_{11} in Fig. 8 - inter-layer TFS in the direction that is perpendicular to the material layers.

TFS_{il} - the maximum of σ_{nn} in Fig. 8 - in-layer TFS in transversely isotropic material layers.

SFS_{ls} - the maximum of σ_{n1} in Fig. 8 - shear failure strength in the plane that is perpendicular to the material layer (longitudinal shear).

SFS_{ts} - the maximum of σ_{nt} in Fig. 8 - shear failure strength in the plane that is parallel to the material layer (transverse shear).

Considering a quadratic approximation (which will be shown to be quite accurate), $I_5^{\mathrm{t\sim i}}$ should not appear in the failure model. Therefore, the general quadratic approximation of failure

for transversely isotropic materials can be expressed as,

$$e_1 \cdot I_1^{t\sim i} + f_1 \cdot \left(I_1^{t\sim i}\right)^2 + e_2 \cdot I_2^{t\sim i} + f_2 \cdot \left(I_2^{t\sim i}\right)^2 + g_{12} \cdot I_1^{t\sim i} \cdot I_2^{t\sim i} + e_3 \cdot I_3^{t\sim i} + e_4 \cdot I_4^{t\sim i} = 1 \quad (9)$$

where e_1, e_2, e_3, e_4, f_1, f_2 and g_{12} are the parameters which need to be determined thereinafter.

Combining Eq. (4) ~ Eq. (7) and Eq. (9), the following equation can be obtained under pure transverse shear condition.

$$e_3 = \frac{1}{SFS_{ts}^2} \quad (10)$$

Combining Eq. (4) ~ Eq. (7) and Eq. (9), the following equation can be obtained under pure longitudinal shear condition.

$$e_4 = \frac{1}{SFS_{ls}^2} \quad (11)$$

The phenomena of experimental results show that there are two failure modes: inter-layer failure mode and in-layer failure mode. These two failure modes have been defined in detail in Section 2.3, which can also be seen in Fig. 8.

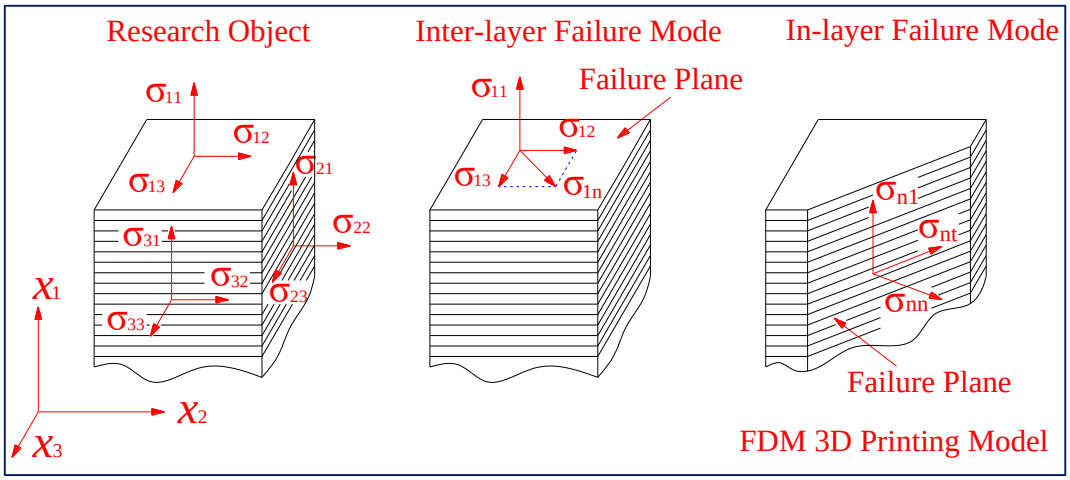

Fig. 8. Schematic of failure modes and failure plane.

3.1.2. Inter-layer failure mode

It is assumed that the failure is caused by the tensile normal stress and shear stresses on the failure plane. For the inter-layer failure mode, the failure plane is x_2-x_3 plane. Therefore, stresses σ_{11} ($\sigma_{11} > 0$), σ_{12} and σ_{13} are considered to result in the inter-layer failure.

277 Combining this assumption and Eq. (9) ~ Eq. (11), the inter-layer failure model can be obtained
278 as follows.

279 $$e_{\mathrm{itl}} \cdot \sigma_{11} + f_{\mathrm{itl}} \cdot \sigma_{11}^2 + \frac{\sigma_{12}^2 + \sigma_{13}^2}{SFS_{\mathrm{ls}}^2} = 1 \tag{12}$$

280 where the parameters have been defined in detail in Section 3.1.1 and Fig. 8. Only e_{itl} and f_{itl}
281 need to be found. A one-dimension uniaxial tensile test can only determine one of the two
282 parameters. Therefore, failure data under a combination of stresses are needed to establish the
283 additional equation for this problem. A large number of experimental data [46-48] have shown
284 that linear term e_{itl} has a very small influence on tensile failure of polymers or composite
285 materials under a quasi-static load and the patterns of failure curves of stresses σ_{11} and σ_{12}
286 (or σ_{13}) are in convex shapes. Therefore, an elliptic equation of σ_{11} and σ_{12} (or σ_{13}) can
287 be used to approximate this tensile failure relationship. With this approximation, the simplified
288 form of Eq. (12) is given below.

289 $$f_{\mathrm{itl}} \cdot \sigma_{11}^2 + \frac{\sigma_{12}^2 + \sigma_{13}^2}{SFS_{\mathrm{ls}}^2} = 1 \tag{13}$$

290 Under these condition, a one-dimension uniaxial tensile test can be used to determine f_{itl}.
291 Thus, Eq. (13) can be reduced to,

292 $$\left(\frac{\sigma_{11}}{TFS_{\mathrm{itl}}} \right)^2 + \frac{\sigma_{12}^2 + \sigma_{13}^2}{SFS_{\mathrm{ls}}^2} = 1 \tag{14}$$

293 where parameters of TFS_{itl} and SFS_{ls} have been defined in detail in Section 3.1.1 and σ_{11},
294 σ_{12}, σ_{13} have been defined in detail in Fig. 8.

295 3.1.3. In-layer failure mode

296 Modelling of the in-layer failure mode is more complicated, since the failure plane is not
297 known in advance. Experimental results obtained during this research show that most of the
298 failure planes of the in-layer failure mode are approximately perpendicular to the material layer.
299 Therefore, a simple case in which the failure plane is perpendicular to the material layer is
300 studied in depth during this research. Again, it is assumed that the failure is caused by the tensile

normal stress and shear stresses on the failure plane. The failure plane is shown in Fig. 8. As defined in Section 3.1.2, stresses σ_{nn} ($\sigma_{nn}>0$), σ_{nt} and σ_{n1} are considered to result in the in-layer failure. Combining this assumption and Eq. (9) ~ Eq. (11), the in-layer failure model can be derived as,

$$e_{il}\cdot\left(\sigma_{22}+\sigma_{33}\right)+f_{il}\cdot\left(\sigma_{22}+\sigma_{33}\right)^2+\frac{\sigma_{23}^2-\sigma_{22}\sigma_{33}}{SFS_{ts}^2}+\frac{\sigma_{12}^2+\sigma_{13}^2}{SFS_{ls}^2}=1 \tag{15}$$

where the parameters have been defined in detail in Section 3.1.1 and Fig. 8. Also only e_{il} and f_{il} need to be found in the above equation. A one-dimensional uniaxial tensile test can only determine one of the two parameters. Therefore, failure data under a combination of stresses are needed to establish the additional equation for this problem. A large number of experimental data [46-48] have shown that the linear term e_{il} has a very small influence on tensile failure of polymers or composite materials under a quasi-static load and the patterns of failure curves of stress σ_{nn} and σ_{nt} (or σ_{n1}) are in convex shapes. Therefore, with the same approximation in Section 3.1.2, the simplified form of Eq. (15) is given below.

$$\left(\frac{\sigma_{22}+\sigma_{33}}{TFS_{il}}\right)^2+\frac{\sigma_{23}^2-\sigma_{22}\sigma_{33}}{SFS_{ts}^2}+\frac{\sigma_{12}^2+\sigma_{13}^2}{SFS_{ls}^2}=1 \tag{16}$$

where parameters of TFS_{il}, SFS_{ts} and SFS_{ls} have been defined in detail in Section 3.1.1. σ_{22}, σ_{33}, σ_{12}, σ_{13} and σ_{23} have been defined in detail in Fig. 8.

3.2. Failure model for plane stress state

3.2.1. Rotation matrix of plane stress state

For transversely isotropic materials including FDM 3D printing materials, the constitutive equation of elastic materials can be expressed in matrix form as,

$$\begin{bmatrix}\varepsilon_1\\ \varepsilon_2\\ \varepsilon_3\\ \varepsilon_4\\ \varepsilon_5\\ \varepsilon_6\end{bmatrix}=\begin{bmatrix}S_{11} & S_{12} & S_{12} & 0 & 0 & 0\\ S_{12} & S_{22} & S_{23} & 0 & 0 & 0\\ S_{12} & S_{23} & S_{22} & 0 & 0 & 0\\ 0 & 0 & 0 & 2\left(S_{22}-S_{23}\right) & 0 & 0\\ 0 & 0 & 0 & 0 & S_{55} & 0\\ 0 & 0 & 0 & 0 & 0 & S_{55}\end{bmatrix}\begin{bmatrix}\sigma_1\\ \sigma_2\\ \sigma_3\\ \sigma_4\\ \sigma_5\\ \sigma_6\end{bmatrix} \tag{17}$$

Eq. (17) can be simplified as Eq. (18) for plane stress state,

$$\begin{bmatrix} \varepsilon_1 \\ \varepsilon_2 \\ \gamma_{12} \end{bmatrix} = \begin{bmatrix} S_{11} & S_{12} & 0 \\ S_{12} & S_{22} & 0 \\ 0 & 0 & S_{55} \end{bmatrix} \begin{bmatrix} \sigma_1 \\ \sigma_2 \\ \tau_{12} \end{bmatrix} \tag{18}$$

where $S_{11}=\frac{1}{E_1}$, $S_{22}=\frac{1}{E_2}$, $S_{55}=\frac{1}{G_{12}}$, $S_{12}=\frac{-\nu_{21}}{E_1}=\frac{-\nu_{12}}{E_2}$. E_1 and E_2 are the Young's moduli in the x_1 and x_2 directions as shown in Fig. 9. G_{12} is the shear modulus in the x_1 - x_2 plane. ν_{21} and ν_{12} are the Poisson's ratios of materials involving directions x_1 and x_2.

Eq. (18) can be expressed in the stiffness matrix form as,

$$\begin{bmatrix} \sigma_1 \\ \sigma_2 \\ \tau_{12} \end{bmatrix} = \begin{bmatrix} Q_{11} & Q_{12} & 0 \\ Q_{12} & Q_{22} & 0 \\ 0 & 0 & Q_{55} \end{bmatrix} \begin{bmatrix} \varepsilon_1 \\ \varepsilon_2 \\ \gamma_{12} \end{bmatrix} \tag{19}$$

The constitutive equation in any direction including on-axis material direction can be expressed as,

$$\begin{bmatrix} \sigma_x \\ \sigma_y \\ \tau_{xy} \end{bmatrix} = \mathbf{T}^{-1} \begin{bmatrix} \sigma_1 \\ \sigma_2 \\ \tau_{12} \end{bmatrix} = \mathbf{T}^{-1}\mathbf{Q} \begin{bmatrix} \varepsilon_1 \\ \varepsilon_2 \\ \gamma_{12} \end{bmatrix} = \mathbf{T}^{-1}\mathbf{Q}\left(\mathbf{T}^{-1}\right)^{\mathrm{T}} \begin{bmatrix} \varepsilon_x \\ \varepsilon_y \\ \gamma_{xy} \end{bmatrix} \tag{20}$$

The rotation matrix $\mathbf{T}$ in Eq. (20) can be expressed as,

$$\mathbf{T} = \begin{bmatrix} \cos^2\theta & \sin^2\theta & 2\sin\theta\cos\theta \\ \sin^2\theta & \cos^2\theta & -2\sin\theta\cos\theta \\ -\sin\theta\cos\theta & \sin\theta\cos\theta & \cos^2\theta-\sin^2\theta \end{bmatrix} \tag{21}$$

where θ is the angle between the material x_1 axis and the global x axis, as shown in Fig. 9.

3.2.2. Failure model

As mentioned before, 3D printing technology is often dedicated to fabricating complex thin-walled structures. Therefore, the cases of plane stress state are very important and thus should be studied thoroughly. For this purpose, two coordinate systems should be built. System x - y - z which represents the load directions is the global coordinate system. System x_1 - x_2 - x_3 which represents the material direction is the material coordinate system. The plane x_2 -

342 x_3 is the material layer plane and the direction x_1 is the direction that is perpendicular to the
343 material layer in the local material coordinate system.
344 The specimens under tension during this research can be simplified as in a plane stress state
345 because of the dimension of the specimens. The global coordinate and the material coordinate
346 systems in 2D are shown in Fig. 9. Therefore, the mechanical theory of plane stress state can
347 be used in the separate-modes of transversely isotropic failure model established in Section 3.1.

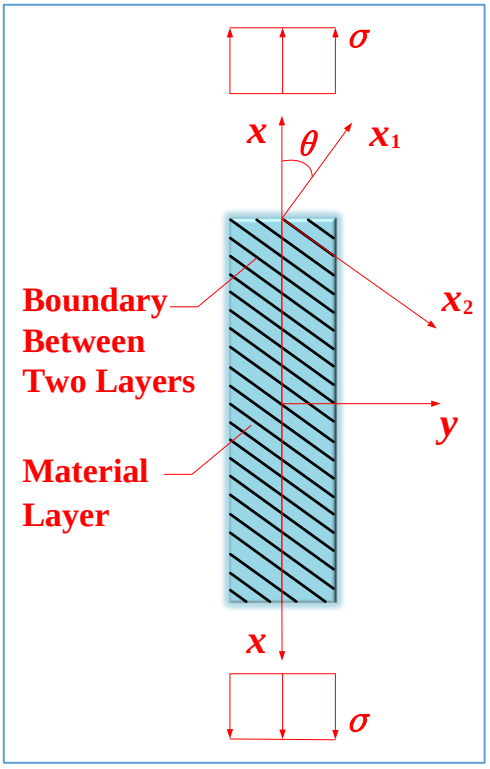

348
349 **Fig. 9.** Material direction and stress direction of FDM 3D printing materials
350 for plane stress state.
351 The non-vanishing stress components in Eq. (14) and Eq. (16) under plane stress state are
352 σ_{11}, σ_{22} and σ_{12} (see Fig. 8). Then the separate-modes of transversely isotropic failure
353 model for plane stress state can be derived as,
354 **Inter-layer Failure Mode**
355
$$\left(\frac{\sigma_{11}}{TFS_{\text{itl}}}\right)^2+\left(\frac{\sigma_{12}}{SFS_{\text{ls}}}\right)^2=1 \tag{22}$$

356 **In-layer Failure Mode**

$$\left(\frac{\sigma_{22}}{TFS_{\mathrm{il}}}\right)^2+\left(\frac{\sigma_{12}}{SFS_{\mathrm{ls}}}\right)^2=1 \tag{23}$$

If only uniaxial stress σ is applied on the specimen shown in Fig. 9, the stress components in the material coordinate system are,

$$\begin{cases}\sigma_{11}=\sigma\cdot\cos^2\theta\\ \sigma_{22}=\sigma\cdot\sin^2\theta\\ \sigma_{12}=-\sigma\cdot\sin\theta\cdot\cos\theta\end{cases} \tag{24}$$

These lead to Inter-layer Failure Mode below

$$\sigma_{\mathrm{itl}}=T_\theta=\left[\frac{\cos^4\theta}{TFS_{\mathrm{itl}}^2}+\frac{\cos^2\theta\cdot\sin^2\theta}{SFS_{\mathrm{ls}}^2}\right]^{-\frac{1}{2}} \tag{25}$$

$\sigma_{\mathrm{itl}}=T_\theta$ is the TFS in the x direction ($\sigma_{\mathrm{itl},\,0}=T_0=TFS_{\mathrm{itl}}$).

Similarly, Eq. (24) leads to In-layer Failure Mode below

$$\sigma_{\mathrm{il}}=T_\theta=\left[\frac{\sin^4\theta}{TFS_{\mathrm{il}}^2}+\frac{\sin^2\theta\cdot\cos^2\theta}{SFS_{\mathrm{ls}}^2}\right]^{-\frac{1}{2}} \tag{26}$$

$\sigma_{\mathrm{il}}=T_\theta$ is the TFS in the x direction ($\sigma_{\mathrm{il},\,90}=T_{90}=TFS_{\mathrm{il}}$).

4. Separation angle

A separate-modes of transversely isotropic theoretical failure model for plane stress state has been established in Eq. (25) and Eq. (26). However, which equation should be used to predict the TFS is still unknown. In order to characterise failure modes properly, the concept of separation angle θ_{SA} which is the demarcation point between the two failure modes is put forward. Let σ_{itl} in Eq. (25) equal to σ_{il} in Eq. (26). Then the following equation for separation angle θ_{SA} is obtained.

$$\left[\frac{\cos^4\theta_{\mathrm{SA}}}{TFS_{\mathrm{itl}}^2}+\frac{\cos^2\theta_{\mathrm{SA}}\cdot\sin^2\theta_{\mathrm{SA}}}{SFS_{\mathrm{ls}}^2}\right]^{-\frac{1}{2}}=\left[\frac{\sin^4\theta_{\mathrm{SA}}}{TFS_{\mathrm{il}}^2}+\frac{\sin^2\theta_{\mathrm{SA}}\cdot\cos^2\theta_{\mathrm{SA}}}{SFS_{\mathrm{ls}}^2}\right]^{-\frac{1}{2}} \tag{27}$$

Simplification of Eq. (27) leads to

$$\tan\theta_{\mathrm{SA}}=\sqrt{\frac{TFS_{\mathrm{il}}}{TFS_{\mathrm{itl}}}} \tag{28}$$

Based on the above theoretical derivation and the phenomena of experimental results

obtained in this research, the following two conclusions can be easily obtained:

(a) When $\theta \leq \theta_{SA}$, the inter-layer failure mode in Eq. (22) or Eq. (25) should be used to predict the TFS of specimens during this research.

(b) When $\theta > \theta_{SA}$, the in-layer failure mode in Eq. (23) or Eq. (26) should be used to predict the TFS of specimens during this research.

5. Results and discussions

5.1. Experimental data

TFS test data for the FDM 3D printing PLA material with all three layer thicknesses are given in Table 3. The magnitude of all these TFS test data is similar to the test results in previous researches [49, 50]. In Table 3, STDEV is Standard Deviation and CV is Coefficient of Variation. T_0, T_{45} and T_{90} represent TFS of the material with 0°, 45° and 90° printing angles, respectively. Based on the discussion in Section 4, T_0 is the inter-layer TFS (TFS_{itl}) and T_{90} is the in-layer TFS (TFS_{il}). TFS of off-axis specimens T_{45} is used to calculate the longitudinal shear failure strength SFS_{ls}. Then, all the parameters in the theoretical failure model for plane stress state in Eq. (25) and Eq. (26) are obtained and TFS of material with other 4 printing angles can be predicted.

Table 3 TFS test data for FDM 3D printing PLA material (unit: MPa).

θ	Test 1	Test 2	Test 3	Test 4	Mean	STDEV	CV (%)
	Layer thickness = 0.1 mm						
0° (T_0)	28.67	25.07	26.21	27.66	26.90	1.58	5.89
45° (T_{45})	30.84	32.97	32.94	28.54	31.32	2.11	6.72
90° (T_{90})	54.37	55.97	57.24	-	55.86	1.44	2.57
	Layer thickness = 0.2 mm						
0° (T_0)	25.53	24.95	26.20	23.05	24.93	1.35	5.43
45° (T_{45})	31.47	30.56	30.02	-	30.68	0.73	2.39

90° (T_{90})	51.18	53.53	54.53	57.65	54.22	2.68	4.95
Layer thickness = 0.3 mm							
0° (T_0)	23.56	24.14	23.63	-	23.78	0.32	1.33
45° (T_{45})	29.32	29.19	28.98	-	29.16	0.17	0.59
90° (T_{90})	44.94	45.62	45.24	48.71	46.13	1.74	3.78

At the same time, Young's modulus and maximum elongation test data (extensometer) for the FDM 3D printing PLA material are given in Table 4.

Table 4 Young's modulus and maximum elongation test data for FDM 3D printing PLA material.

θ	Young's modulus (unit: MPa)			maximum elongation (%)		
	Mean	STDEV	CV(%)	Mean	STDEV	CV
Layer thickness = 0.1 mm						
0°	1528.75	31.04	2.03	2.09	0.13	6.15
45°	1555.33	28.04	1.80	2.39	0.14	5.85
90°	1648.67	53.70	3.26	3.87	0.11	2.90
Layer thickness = 0.2 mm						
0°	1951.50	53.73	2.75	1.59	0.10	6.32
45°	2065.33	74.66	3.61	1.88	0.09	4.87
90°	2251.04	58.93	2.62	2.81	0.11	3.74
Layer thickness = 0.3 mm						
0°	1660.67	86.63	5.22	1.75	0.09	5.12
45°	1769.67	82.42	4.66	2.05	0.12	5.90
90°	1726.50	32.93	1.91	3.14	0.08	2.57

5.2. Discussion of separation angle θ_{SA}

Based on the experimental data in Section 5.1 and the expression of separation angle in Eq. (28), separation angle θ_{SA} can be easily obtained, and are given in Table 5. Its values ranges between 45° and 60°.

Table 5 Separation angle for the FDM 3D printing PLA material.

Layer thickness (mm)	θ_{SA} (°)
0.1	55.24
0.2	55.85
0.3	54.32

As explained therein before, there are two failure modes, which can be seen in Fig. 10 ~ Fig. 12. In addition, the experimental results of separation angles θ_{SA} are given. Almost all the separation angles θ_{SA} of experimental results are between 45° and 60°, which is basically consistent with theoretically predicted value in Table 5. Therefore, one can conclude that the theoretical model established in Section 4 has the capacity in predicting the approximate range of the separation angle θ_{SA}.

The classification of failure modes is given in Table 6. Almost all the inter-layer failure events occur when the printing angles are 0°, 15°, 30° and 45°. In contrast, in-layer failure events occur when the printing angles are 60°, 75° and 90°. So the conclusion that inter-layer failure tends to occur when the printing angle is small and in-layer failure tends to occur when the printing angle is big can be drawn.

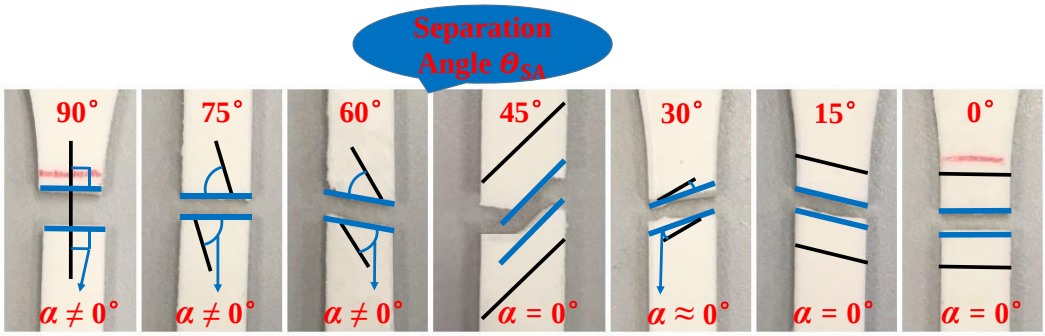

(a) Separation angle θ_{SA} of test-1.

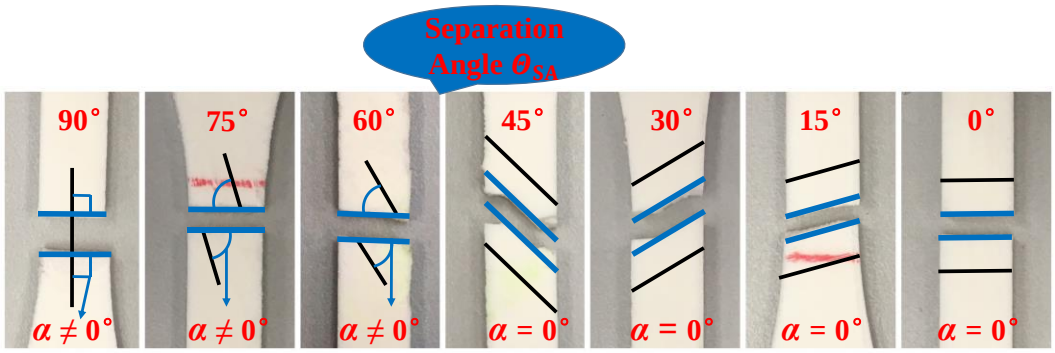

(b) Separation angle θ_{SA} of test-2.

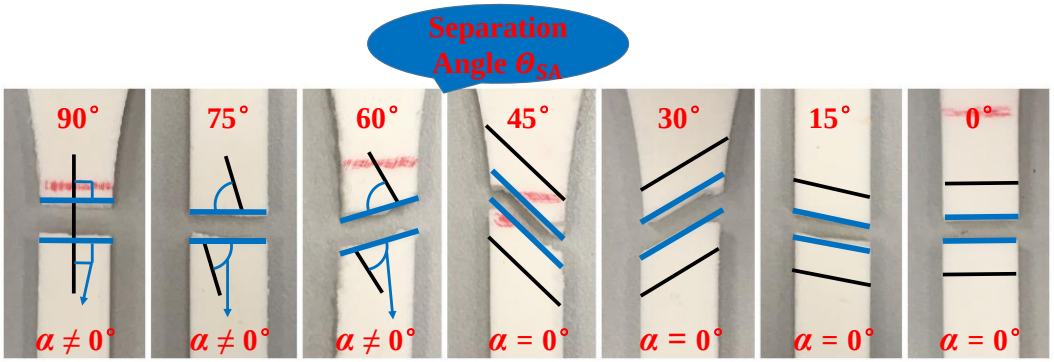

(c) Separation angle θ_{SA} of test-3.

Fig. 10. Distribution of separation angle θ_{SA} with 0.1mm layer thickness.

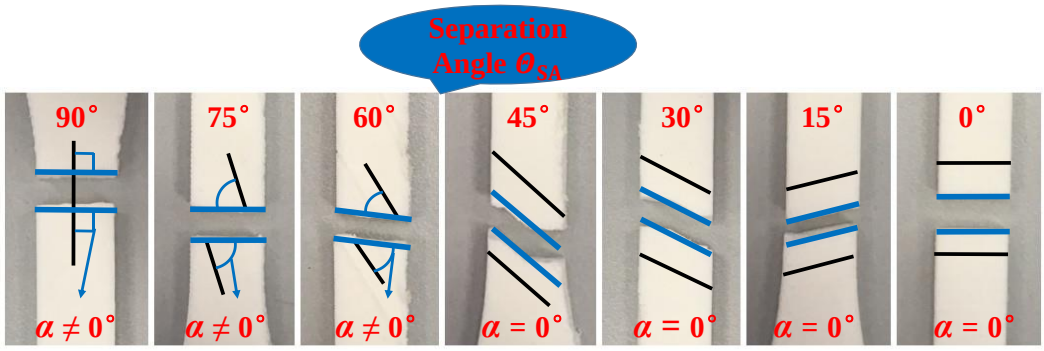

(a) Separation angle θ_{SA} of test-1.

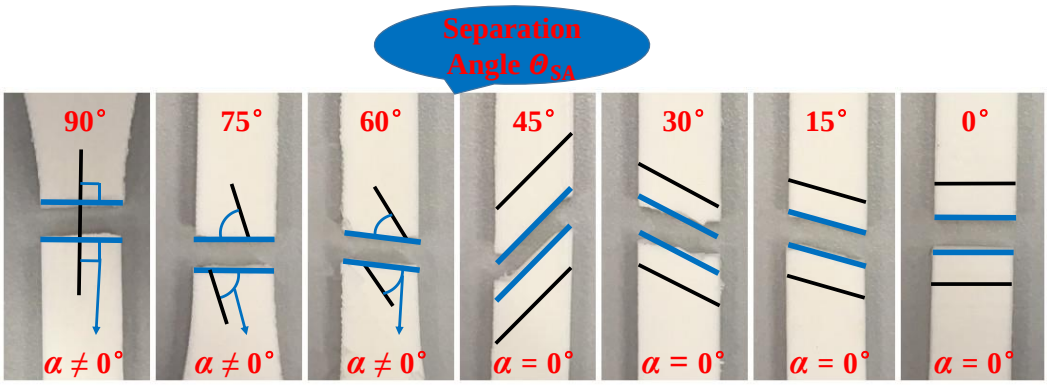

(b) Separation angle θ_{SA} of test-2.

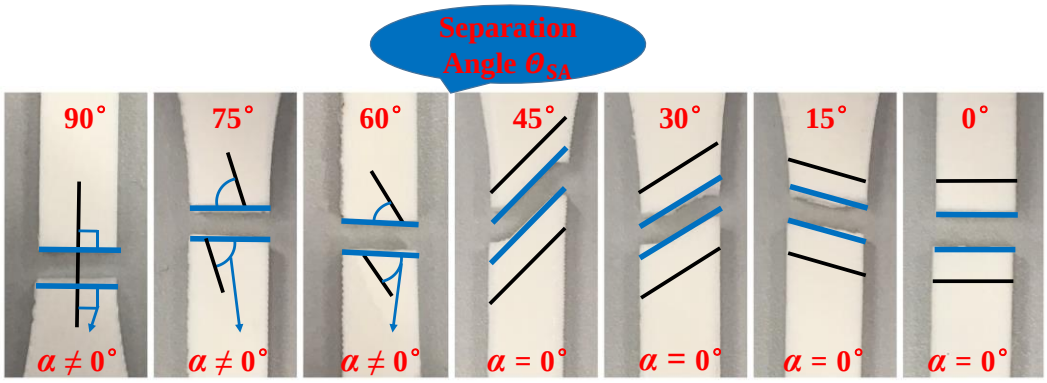

(c) Separation angle θ_{SA} of test-3.

Fig. 11. Distribution of separation angle θ_{SA} with 0.2mm layer thickness.

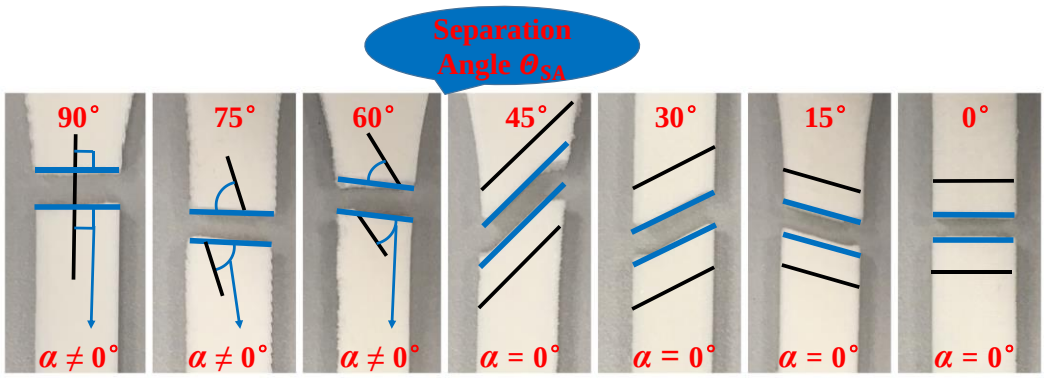

(a) Separation angle θ_{SA} of test-1.

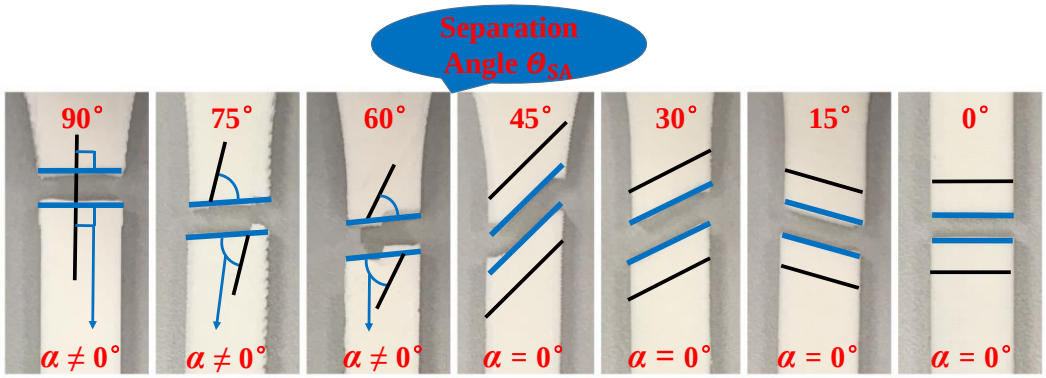

(b) Separation angle θ_{SA} of test-2.

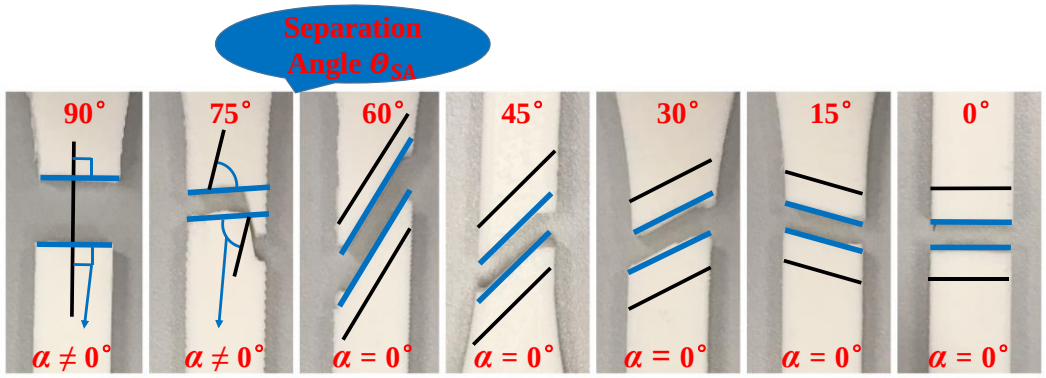

(c) Separation angle θ_{SA} of test-3.

Fig. 12. Distribution of separation angle θ_{SA} with 0.3mm layer thickness.

Table 6 The classification of failure modes.

Layer thickness (mm)	Test times	Failure modes	
		Inter-layer failure	In-layer failure
0.1	1	0°, 15°, 30°, 45°	60°, 75°, 90°
	2	0°, 15°, 30°, 45°	60°, 75°, 90°
	3	0°, 15°, 30°, 45°	60°, 75°, 90°
0.2	1	0°, 15°, 30°, 45°	60°, 75°, 90°
	2	0°, 15°, 30°, 45°	60°, 75°, 90°
	3	0°, 15°, 30°, 45°	60°, 75°, 90°
0.3	1	0°, 15°, 30°, 45°	60°, 75°, 90°

	2	0°, 15°, 30°, 45°	60°, 75°, 90°
	3	0°, 15°, 30°, 45°, 60°	75°, 90°

5.3. Comparison between theoretical results and experimental data for TFS

TFS comparison between theoretical results and experimental data is made in Fig. 13. In these three figures, the data including theoretical results and experimental data with STDEV continues to increase with the printing angle increasing from 0° to 90°. This change rule can also be seen in previous studies [50, 51]. At the same time, the degree of agreement between theoretical results and experimental data is satisfactory.

In order to quantify the prediction accuracy of the theoretical model, a Generalized-Relative-Root-Mean-Square Error (*GRRMSE*) between theoretical results and experimental data is defined in Eq. (29). When the *GRRMSE* is close to zero, the accuracy of the theoretical model is high. In Table 7, the order of magnitude of all the *GRRMSE* is 10^{-2}, which is consider to be very close to zero. The same results can also be seen in Fig. 14. Therefore, one can confirm that the theoretical model established in this paper has the capacity in predicting the TFS of FDM 3D printing PLA material with different printing angles.

$$GRRMSE = \frac{\sqrt{\frac{1}{n}\cdot\sum_{i=1}^{n}(\mathrm{TR}_i - \mathrm{ED}_i)^2}}{\frac{1}{n}\cdot\sum_{i=1}^{n}\mathrm{ED}_i} \tag{29}$$

where n is the number of distinct printing angle (n = 7 in this research),

TR_i refers to theoretical results corresponding to the ith printing angle, and

ED_i refers to averaged experimental data corresponding to the ith printing angle.

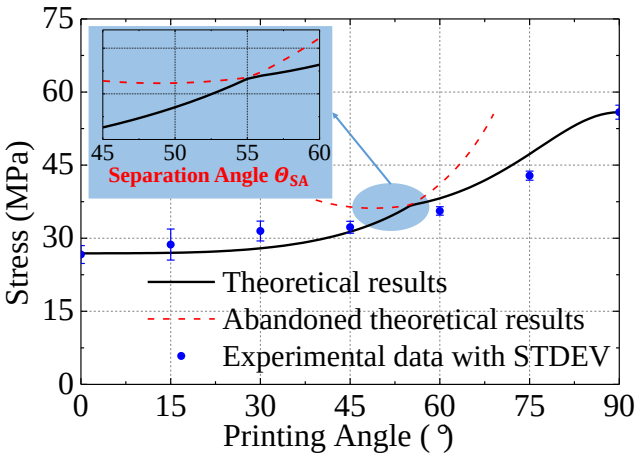

(a) Comparison of 0.1 mm layer thickness.

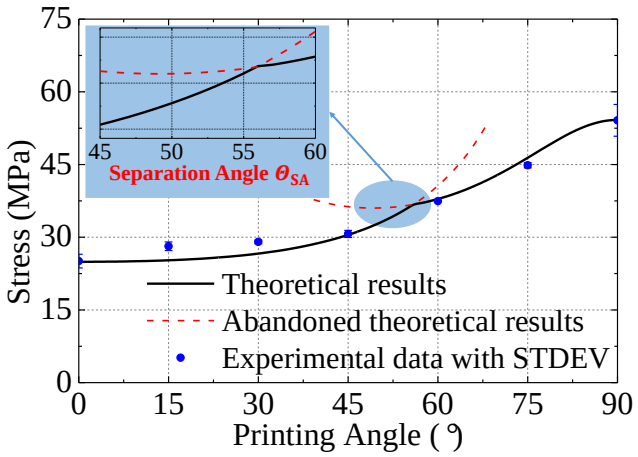

(b) Comparison of 0.2 mm layer thickness.

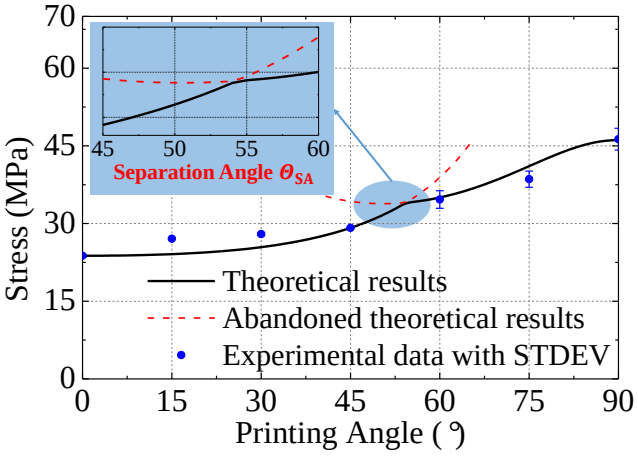

(c) Comparison of 0.3 mm layer thickness.

Fig. 13. TFS comparison between theoretical results and experimental data.

Table 7 *GRRMSE* between theoretical results and experimental data.

Layer thickness (mm)	*GRRMSE*
0.1	0.0684

0.2	0.0436
0.3	0.0544

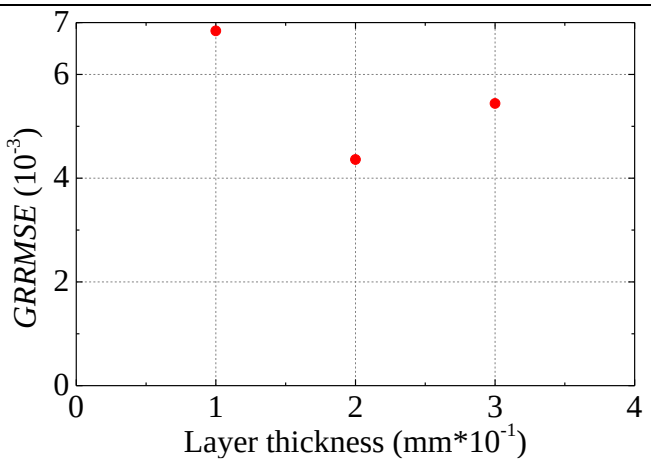

Fig.14. *GRRMSE* between theoretical results and experimental data.

5.4. Influence of layer thickness on TFS

The reliability of the theoretical model established during this research has been verified in Section 5.3. So the theoretical model can be used to analyse the influence of layer thickness on TFS. Fig. 15 displays this influence. Obviously, the TFS of the FDM 3D printing PLA material with same printing angle becomes bigger as layer thickness decreases from 0.3 mm to 0.1 mm. In Fig. 15, one can also see that the separation angle range of the FDM 3D printing PLA material stays between 45° and 60°.

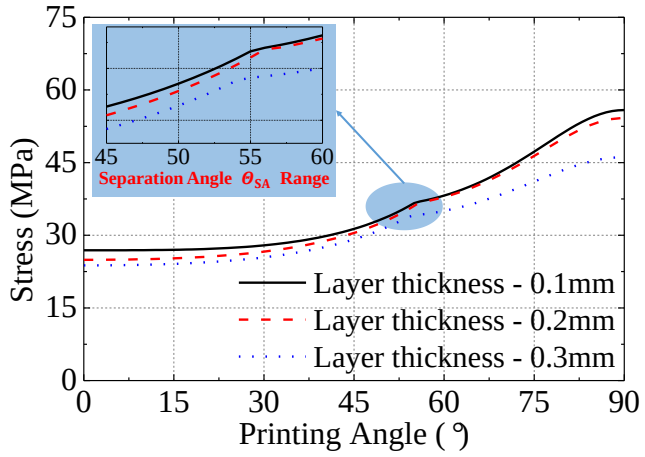

Fig. 15. Influence of layer thickness on TFS.

6. Conclusions

A preliminary study of tensile failure strength and the associated separation angle θ_{SA} of

a FDM (Fused Deposition Modelling) 3D printing PLA (polylactic acid) material is presented in this paper. It is found that the material can be modelled as transversely isotropic and a separate-modes of transversely isotropic theoretical failure model is put forward and then verified by experimental data, as well as the range of separation angle θ_{SA} of this material. Based on the results and analysis of this research, four conclusions can be drawn as follows.

1. All the Generalized-Relative-Root-Mean-Square Error (*GRRMSE*) between theoretical results and experimental data are close to zero. So the theoretical model based on the transversely isotropic material hypothesis and separate failure-modes hypothesis established in this research is suitable for the failure of FDM 3D printing PLA material and has the capacity in predicting the tensile failure strength of this material.

2. The experimental results show that the range of separation angle θ_{SA} is between 45° and 60°. The theoretical model is shown to be able to approximately predict the range of separation angle θ_{SA} of this FDM 3D printing PLA material.

3. Two different failure modes are discovered in the tensile experiments. Inter-layer failure mode occurs when the printing angle is small while in-layer failure mode occurs when the printing angle is big.

4. Apparently, the tensile failure strength of this FDM 3D printing PLA material with the same printing angles becomes bigger as its layer thickness decreases from 0.3 mm to 0.1 mm.

Further research will be concentrated on optimizing the separate-modes of transversely isotropic theoretical failure model. The theoretical model will be extended to predict the failure strength and distribution of separation angle (θ_{SA}) of different kinds of 3D printing materials.

Acknowledgements

This work was supported by the National Key R&D Program of China (2017YFB1102801), and the Graduate Innovation Team Foundation of Northwestern Polytechnical University. Part of the theoretical work is carried out during the visit by the first author to the University of Liverpool.

References

[1] Wang X, Jiang M, Zhou Z, Gou J, Hui D. 3D printing of polymer matrix composites: A review and prospective. Composites Part B: Engineering. 2017; 110: 442-58.

[2] Parandoush P, Lin D. A review on additive manufacturing of polymer-fiber composites. Compos Struct 2017; 182: 36–53.

[3] Ngo TD, Kashani A, Imbalzano G, Nguyen KTQ, Hui D. Additive manufacturing (3D printing): A review of materials, methods, applications and challenges. Compos Part B Eng 2018; 143: 172–96.

[4] Zhang Z, Wang B, Hui D, Qiu J, Wang S. 3D bioprinting of soft materials-based regenerative vascular structures and tissues. Compos Part B Eng 2017; 123: 279–91.

[5] Gibson I, Rosen DW, Stucker B. Additive manufacturing technologies: Springer; 2014.

[6] Wimpenny DI, Pandey PM, Jyothish Kumar L. Advances in 3D Printing & additive manufacturing technologies. 2017.

[7] Xu XJ, Zheng ML, Wang XC. On vibrations of nonlocal rods: Boundary conditions, exact solutions and their asymptotics. Int J Eng Sci 2017; 119: 217–31.

[8] Zhang K, Ge MH, Zhao C, Deng ZC, Xu XJ. Free vibration of nonlocal Timoshenko beams made of functionally graded materials by Symplectic method. Compos Part B Eng 2019; 156: 174–84.

[9] Amirpour M, Bickerton S, Calius E, Das R, Mace B. Numerical and experimental study on deformation of 3D-printed polymeric functionally graded plates: 3D-Digital Image Correlation approach. Compos Struct 2019; 211: 481–9.

[10] Mansouri MR, Montazerian H, Schmauder S, Kadkhodapour J. 3D-printed multimaterial composites tailored for compliancy and strain recovery. Compos Struct 2018; 184: 11–7.

[11] Stepashkin, Chukov DI, Senatov FS, Salimon AI, Korsunsky AM, Kaloshkin SD. 3D-printed PEEK-carbon fiber (CF) composites: Structure and thermal properties. Compos Sci Technol 2018; 164: 319–26.

[12] Pyl L, Kalteremidou KA, Van Hemelrijck D. Exploration of the design freedom of 3D printed continuous fibre-reinforced polymers in open-hole tensile strength tests. Compos Sci Technol 2019; 171: 135–51.

530 [13] Tekinalp HL, Kunc V, Velez-Garcia GM, Duty CE, Love LJ, Naskar AK, et al. Highly
531 oriented carbon fiber-polymer composites via additive manufacturing. Compos Sci
532 Technol 2014; 105: 144–50.
533 [14] Berman B. 3-D printing: The new industrial revolution. Bus Horiz 2012; 55: 155–62.
534 [15] Wolfs RJM, Bos FP, Salet TAM. Early age mechanical behaviour of 3D printed concrete:
535 Numerical modelling and experimental testing. Cem Concr Res 2018; 106: 103–16.
536 [16] Panda B, Lim JH, Tan MJ. Mechanical properties and deformation behaviour of early age
537 concrete in the context of digital construction. Compos Part B Eng 2019; 165: 563–71.
538 [17] Talagani M, DorMohammadi S, Dutton R, Godines C, Baid H, Abdi F, et al. Numerical
539 simulation of big area additive manufacturing (3D printing) of a full size car. SAMPE
540 Journal. 2015; 51(4): 27-36.
541 [18] Do AV, Khorsand B, Geary SM, Salem AK. 3D Printing of Scaffolds for Tissue
542 Regeneration Applications. Adv Healthc Mater 2015; 4: 1742–62.
543 [19] Zhu W, Ma X, Gou M, Mei D, Zhang K, Chen S. 3D printing of functional biomaterials
544 for tissue engineering. Curr Opin Biotechnol 2016; 40: 103–12.
545 [20] Wang MO, Vorwald CE, Dreher ML, Mott EJ, Cheng MH, Cinar A, et al. Evaluating 3D-
546 printed biomaterials as scaffolds for vascularized bone tissue engineering. Adv Mater 2014;
547 27: 138–44.
548 [21] Blaeser A, Duarte Campos DF, Puster U, Richtering W, Stevens MM, Fischer H.
549 Controlling Shear Stress in 3D Bioprinting is a Key Factor to Balance Printing Resolution
550 and Stem Cell Integrity. Adv Healthc Mater 2016; 5: 326–33.
551 [22] Godoi FC, Prakash S, Bhandari BR. 3D printing technologies applied for food design:
552 Status and prospects. J Food Eng 2016; 179: 44–54.
553 [23] Sun J, Zhou W, Huang D, Fuh JYH, Hong GS. An Overview of 3D Printing Technologies
554 for Food Fabrication. Food Bioprocess Technol 2015; 8: 1605–15.
555 [24] Lipton JI, Cutler M, Nigl F, Cohen D, Lipson H. Additive manufacturing for the food
556 industry. Trends Food Sci Technol 2015; 43: 114–23.
557 [25] Wang BZ, Chen Y. The effect of 3D printing technology on the future fashion design and
558 manufacturing. Applied Mechanics and Materials: Trans Tech Publ; 2014. p. 2687-91.
559 [26] Yao T, Deng Z, Zhang K, Li S. A method to predict the ultimate tensile strength of 3D

printing polylactic acid (PLA) materials with different printing orientations. Compos Part B Eng 2019; 163: 393-402.

[27] Chacón JM, Caminero MA, García-Plaza E, Núñez PJ. Additive manufacturing of PLA structures using fused deposition modelling: Effect of process parameters on mechanical properties and their optimal selection. Mater Des 2017; 124: 143–57.

[28] Tanikella NG, Wittbrodt B, Pearce JM. Tensile strength of commercial polymer materials for fused filament fabrication 3D printing. Addit Manuf 2017; 15: 40–7.

[29] Sood AK, Ohdar RK, Mahapatra SS. Parametric appraisal of mechanical property of fused deposition modelling processed parts. Mater Des 2010; 31: 287–95.

[30] Croccolo D, De Agostinis M, Olmi G. Experimental characterization and analytical modelling of the mechanical behaviour of fused deposition processed parts made of ABS-M30. Comput Mater Sci 2013; 79: 506–18.

[31] García Plaza E, Núñez López PJ, Caminero Torija MÁ, Chacón Plaza JM. Analysis of PLA geometric properties processed by FFF additive manufacturing: Effects of process parameters and plate-extruder precision motion. Polymers (Basel) 2019; 11.

[32] Ahn SH, Montero M, Odell D, Roundy S, Wright PK. Anisotropic material properties of fused deposition modeling ABS. Rapid Prototyp J 2002; 8: 248–57.

[33] Rayegani F, Onwubolu GC. Fused deposition modelling (fdm) process parameter prediction and optimization using group method for data handling (gmdh) and differential evolution (de). Int J Adv Manuf Technol 2014; 73: 509–19.

[34] Torrado Perez AR, Roberson DA, Wicker RB. Fracture surface analysis of 3D-printed tensile specimens of novel ABS-based materials. J Fail Anal Prev 2014; 14: 343–53.

[35] Sood AK, Ohdar RK, Mahapatra SS. Experimental investigation and empirical modelling of FDM process for compressive strength improvement. J Adv Res 2012; 3: 81–90.

[36] Tymrak BM, Kreiger M, Pearce JM. Mechanical properties of components fabricated with open-source 3-D printers under realistic environmental conditions. Mater Des 2014; 58: 242–6.

[37] Song Y, Li Y, Song W, Yee K, Lee KY, Tagarielli VL. Measurements of the mechanical response of unidirectional 3D-printed PLA. Mater Des 2017; 123: 154–64.

[38] Zhang P, To AC. Transversely isotropic hyperelastic-viscoplastic model for glassy

polymers with application to additive manufactured photopolymers. Int J Plast 2016; 80: 56–74.

[39] Tsai SW, Wu EM. A General Theory of Strength for Anisotropic Materials. J Compos Mater 1971; 5: 58–80.

[40] Ahn SH, Baek C, Lee S, Ahn IS. Anisotropic tensile failure model of rapid prototyping parts - Fused Deposition Modeling (FDM). Int J Mod Phys B 2003; 17: 1510–6.

[41] Obst P, Launhardt M, Drummer D, Osswald P V., Osswald TA. Failure criterion for PA12 SLS additive manufactured parts. Addit Manuf 2018; 21: 619–27.

[42] Ning F, Cong W, Hu Y, Wang H. Additive manufacturing of carbon fiber-reinforced plastic composites using fused deposition modeling: Effects of process parameters on tensile properties. J Compos Mater 2017; 51: 451–62.

[43] Caminero MÁ, Chacón JM, García-Plaza E, Núñez PJ, Reverte JM, Becar JP. Additive manufacturing of PLA-based composites using fused filament fabrication: Effect of graphene nanoplatelet reinforcement on mechanical properties, dimensional accuracy and texture. Polymers (Basel) 2019; 11.

[44] Ulu E, Korkmaz E, Yay K, Burak Ozdoganlar O, Burak Kara L. Enhancing the Structural Performance of Additively Manufactured Objects Through Build Orientation Optimization. J Mech Des Trans ASME 2015; 137: 1–9.

[45] Hashin Z, Rotem A. A Fatigue Failure Criterion for Fiber Reinforced Materials. J Compos Mater 1973; 7: 448–64.

[46] Hashin Z. Failure Criteria for Unidirectional Fiber Composites. Journal of Applied Mechanics. 1980; 47(2): 329-34.

[47] Tao Y, Chen H, Yao K, Lei H, Pei Y, Fang D. Experimental and theoretical studies on inter-fiber failure of unidirectional polymer-matrix composites under different strain rates. Int J Solids Struct 2017; 113–114: 37–46.

[48] Puck A, Schürmann H. Failure analysis of FRP laminates by means of physically based phenomenological models. Fail Criteria Fibre-Reinforced-Polymer Compos 2004; 3538: 832–76.

[49] Goh GD, Yap YL, Tan HKJ, Sing SL, Goh GL, Yeong WY. Process–Structure–Properties in Polymer Additive Manufacturing via Material Extrusion: A Review. Crit Rev Solid State

Mater Sci 2019; 0: 1–21.
[50] Zhao Y, Chen Y, Zhou Y. Novel mechanical models of tensile strength and elastic property of FDM AM PLA materials: Experimental and theoretical analyses. Mater Des 2019; 181: 108089.
[51] Alaimo G, Marconi S, Costato L, Auricchio F. Influence of meso-structure and chemical composition on FDM 3D-printed parts. Compos Part B Eng 2017; 113: 371–80.